CROATICA CHEMICA ACTA
CCACAA, ISSN-0011-1643, ISSN-1334-417X
Croat. Chem. Acta **82** (1) (2009) 105−114.
CCA-3300

Original Scientific Paper

Ultrafast Excited-state Proton Transfer Processes: Energy Surfaces and On-the-fly Dynamics Simulations*

Adélia J. A. Aquino, ** **Felix Plasser, Mario Barbatti, and Hans Lischka****

Institute for Theoretical Chemistry, University of Vienna, Waehringerstrasse 17, A-1090 Vienna, Austria

RECEIVED JULY 7, 2008; REVISED OCTOBER 9, 2008; ACCEPTED OCTOBER 10, 2008

Abstract. The excited-state intramolecular proton transfer (ESIPT) is reviewed for several benchmark systems [*o*-hydroxybenzaldehyde (OHBA), salicylic acid and 2-(2′-hydroxyphenyl)-benzothiazole (HBT)] in order to verify the applicability of the time-dependent density functional theory (TDDFT) and the resolution-of-the-identity approximate second-order coupled cluster (RI-CC2) methods. It was found that these approaches are very well suited for the description of ESIPT processes. A comparative investigation of previous and new excited-state dynamics simulations is performed for HBT, 10-hydroxybenzo[*h*]quinoline (HBQ), and [2,2′-bipyridyl]-3,3′-diol ($BP(OH)_2$). The time scale for the ESIPT process in these systems ranges in the time interval of 30−40 fs for HBT and HBQ and amounts to about 10 fs for the first proton transfer step in $BP(OH)_2$. The dynamics simulations also show that the proton transfer in HBT is strongly supported by skeletal modes and the proton plays a rather passive role, whereas in HBQ a semi-passive mechanism is found due to its increased rigidity in comparison to HBT. The special role of the double proton transfer in $BP(OH)_2$ is discussed as well.

Keywords: density functional theory, on-the-fly dynamics, excited states, proton transfer mechanism

INTRODUCTION

Proton transfer belongs to one of the most basic structural changes occurring in chemical and biological processes. A very fascinating field is the intramolecular proton transfer in excited states (ESIPT) since acidity and basicity relations in an intramolecular hydrogen bond can be significantly altered upon electronic excitation. Such processes are not only of highest scientific interest but have also considerable practical importance because many of the organic substances investigated can be used as photostabilizers,[1,2] sun blockers, laser dyes[3−5] and metal ion sensors.[6] For that reason, a large number of experimental[7−14] and theoretical[4,15−25] studies on the ESIPT have been performed for a large variety of systems.

ESIPT represents a phototautomerization process, namely, the conversion from an excited-enol (E^*) to an excited-keto (K^*) structure along a pre-existing hydrogen bond as illustrated in Scheme 1. This process has been found in many cases to proceed exceptionally fast at a subpicosecond time scale.[26−29] In most cases where ESIPT is observed, the proton donor consists of a hydroxyl group and the acceptor is a nitrogen atom or a carbonyl group. Eventually, the excited keto structure decays to the ground state either by radiative (fluorescence) or nonradiative (internal conversion) processes, which can be followed by a reverse proton transfer, returning to the original ground state enol structure.

The excited keto tautomer produced by the ESIPT usually shows significant differences in geometric structure and electronic configuration in comparison to the original enol species. This fact leads to large Stokes shifts of the order of 8 000 to 10 000 cm^{-1}. This remarkable property has always attracted strong interest in ESIPT systems and has led to many important applications as already mentioned above. The intramolecular character of ESIPT allows its investigation under well characterized conditions using stationary spectroscopic

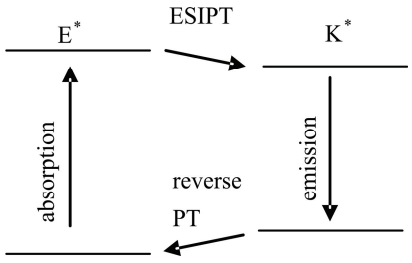

Scheme 1. Illustration of a typical ESIPT photocycle.

* Dedicated to Professor Zvonimir Maksić on the occasion of his 70th birthday.
** Authors to whom correspondence should be addressed. (E-mail: adelia.aquino@univie.ac.at; hans.lischka@univie.ac.at)

methods or time-resolved pump-probe experiments with exceptionally high accuracy.[13,30]

Theoretical studies of ESIPT in large systems are particularly demanding. Multireference methods such as complete active space self-consistent field (CASSCF) and complete active space perturbation theory to second order (CASPT2),[31,32] multireference configuration interaction with singles and doubles (MR-CISD) and multireference averaged quadratic coupled cluster (MR-AQCC)[33,34] methods have been used in the investigation of excited states. These methods, however, are computationally too demanding for most of the interesting molecules showing ESIPT. DFT methods are conceptually much easier and considerably less challenging than the just mentioned multi-configurational approaches. In recent years, with the development of the variational formulation[35] of time-dependent density functional theory (TDDFT) substantial progress has been accomplished in the calculation of analytic energy gradients of excited states. Nevertheless, its usage has to be carefully checked case by case due the possibility of a wrong description of charge transfer states. The resolution-of the-identity approximate second-order coupled cluster (RI-CC2)[36–38] method is an interesting alternative to study excited states. The RI method speeds up the calculations considerably being, therefore, very useful for the calculations of large molecules. Although this method is still computationally much more demanding than TDDFT, it is not subject to the just-mentioned problems in the charge-transfer state description. For this reason, RI-CC2 will be used here as the primary source for accurate benchmark calculations in comparison to TDDFT results. Nevertheless, neither the TDDFT nor the RI-CC2 methods are appropriate for the treatment of regions having strong multireference character as those close to conical intersections, which are particularly relevant for molecules showing high internal conversion rates after the ESIPT.

In recent years, our group has carried out theoretical investigations for several ESIPT systems[39–42] including medium-sized molecules such as malonaldehyde (MA), *o*-hydroxybenzaldehyde (OHBA), salicylic acid (SA), 7-hydroxy-1-indanone (7HIN), and larger systems such as 2-(2′-hydroxyphenyl) benzothiazole (HBT) and 10-hydroxybenzo[*h*]quinoline (HBQ). In this work, we review our main results and perform comparative investigations of a subset of those systems, namely, SA, HBT OHBA, HBQ, and $BP(OH)_2$, all of them illustrated in Scheme 2. In addition, new results for [2,2'-bipyridyl]-3,3'-diol [$BP(OH)_2$], a system for which single- and double proton transfer processes can occur in competition to each other, are also reported.

One main aspect of the present discussions is the selection and justification of methods to be used in "on-the-fly" dynamics simulations[43–45] in excited states. Such dynamics investigations can provide details of photochemical reactions including molecular mechanisms and time scales. They are, however, extremely time consuming and the computational methods have to be selected carefully balancing computational efficiency and accuracy. The reported dynamics simulations concentrate on HBT, and HBQ and $BP(OH)_2$ for which the ESIPT will be discussed in detail.

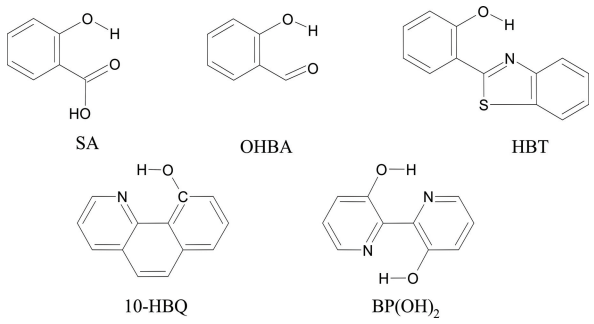

Scheme 2. Investigated molecules.

COMPUTATIONAL DETAILS

This section is divided into subsections providing the technical information for each set of calculations reported throughout this work.

Proton Transfer Reaction Paths

The coordinate-driven minimum-energy path approach was chosen to build the ESIPT reaction paths. The reaction coordinate is defined as[31]

$$R_{-} = 1/2\left(R_{\mathrm{OH}} - R_{\mathrm{XH}}\right) \tag{1}$$

where X stands for the proton acceptor atoms oxygen or nitrogen. The paths were computed by relaxing all other internal coordinates for each fixed value of R_{OH}.

All calculations were performed using the TDDFT[35,46,47] and RI-CC2[37,38] approaches. For the TDDFT calculations two functionals, B3LYP[48] and PBE[49] were used. The SVP,[50] TZVP[51] and TZVPP[51]basis sets consisted of split-valence and triple-ξ quality, respectively. C_s symmetry was adopted for the nuclear framework and all stationary points were confirmed by harmonic frequency analysis.

The radiative decay times (in au) were computed according to[52]

$$\tau = \frac{c^3}{2\left(\Delta E\right)^2 f} \tag{2}$$

where c is the velocity of light, ΔE is the transition energy and f represents the oscillator strength.

Potential Energy Surfaces and Excited-state Classical Dynamics for HBT, 10-HBQ and $BP(OH)_2$

Geometry optimizations as well as computation of vertical and adiabatic excitations were performed by means of the TDDFT/B3LYP and RI-CC2 methods. The SVP[50] basis set was used and C_s symmetry restrictions in the nuclear framework were applied to all static calculations. The SVP basis set is sufficiently small but flexible enough to allow for cost-effective calculations on larger systems, as is the case for HBT and HBQ. The calculations for $BP(OH)_2$ were performed using the TZVP[51] and SVP-SV [50] basis sets. The label SVP-SV indicates the use of the SVP basis for heavy and hydrogen atoms involved in hydrogen bonds and SV for the remaining hydrogen atoms. Equilibrium points were characterized by a harmonic analysis.

Classical dynamics simulations were carried out for HBT, HBQ and $BP(OH)_2$ on the energy surface of the first excited singlet state S_1. Newton's equations for the nuclear motion were solved by means of the Velocity-Verlet algorithm with a time step of 0.5 fs. An "on-the-fly" technique is used computing electronic energies and analytic energy gradients at each time step as needed using the TDDFT/B3LYP/SVP-SV method. The initial conditions for nuclear coordinates and momenta in the dynamics simulations were generated from a Wigner distribution of the ground-state quantum harmonic-oscillator in the electronic ground state.[43,44] All TDDFT and RI-CC2 calculations were performed with the TURBOMOLE program system.[53] Dynamics simulations were performed using the NEWTON-X program system.[44,54]

RESULTS AND DISCUSSION

Static Analysis of the ESIPT

As already mentioned, MA, OHBA, 7-HIN, SA and HBT were selected for the investigation of the applicability of TDDFT to describe ESIPT using the B3LYP and PBE functionals. Only the enol form was found as energy minimum in the ground state for all of these compounds. Searches for a keto minimum in the ground state starting from the S_1 keto structure were also undertaken. Nevertheless, the optimization procedure always led directly to the enol form without energy barrier. The conclusion from this finding is that after transition from S_1 (keto) to S_0 there will be a barrierless path to the S_0 (enol) minimum. Nevertheless, if the keto form undergoes further ultrafast transformation in the S_1 state, as has been demonstrated explicitly for 2-(2'-hydroxyphenyl)benzotriazole HBT[41,55] also other regions of the S_0 energy surface will be reached leading to interring *cis-trans* isomerization.

Extensive calculations using several methods and basis sets have been performed for vertical, adiabatic (minimum to minimum and with inclusion of zero-point energy corrections), vertical fluorescence transitions (fl) and Stokes shift (st) for the ππ* and nπ* excited states. The Stokes shift is computed as the difference between the vertical excitation and the fluorescence energy. Besides comparisons of results obtained with different methods (see below) the question of the character of the S_1 state and its separation from the S_2 state is of interest since it will decide whether the dynamics simulations can be performed adiabatically on a single energy surface. The analysis of results given in Ref. 39 shows that for the vertical excitation in OHBA (enol form) the S_1 and S_2 states are located closely together within 0.05 eV and that the S_1 state has ππ* character. The same is true for the keto S_1 and S_2 structures. In case of SA the vertical excitation to the nπ* state is significantly higher than that to the ππ* state. Geometry optimization (keto* minima) lead to a closer approach of both states, but even there the ππ* state is lower than the nπ* state by about 0.2 eV. This trend is similar in HBT and is strongly enhanced in HBQ.[40] Thus, as expected, with increasing π conjugation the ππ* state is stabilized in comparison to the nπ* state. Nevertheless, it can be expected that even for systems like HBT and $BP(OH)_2$ the latter state can assume some importance. Relatively rare cases of switches between both states have been observed in the $BP(OH)_2$ dynamics and also the proton transfer curves given in Ref. 39 indicate such switches. In total we conclude that for systems such as HBT and $BP(OH)_2$ the adiabatic treatment of the ESIPT in the S_1 state is reasonable but that the effect of the nπ* state should not be neglected. Such switches between both states are, in fact, permitted in the dynamics calculations described below.

The following comparison of computational methods is restricted to the S_1 state. Results are summarized in Tables 1 and 2 for OHBA, SA, HBT and HBQ. Similar trends can be observed in all cases. B3LYP and RI-CC2 vertical excitation energies agree quite well with both experimental and available CASPT2 results, with B3LYP performing somewhat better. The PBE excitation energies are generally too low, especially in the case of the transition energy to the nπ* state. The adiabatic (minimum to minimum) transition energies are decreased by about 0.4−0.5 eV as compared to the vertical excitation. The effect of the zero-point energy correction (not shown) is about 0.1 eV. The basis set influence is very small in the TDDFT case and amounts to about 0.1 eV for RI-CC2. The fluorescence results for

Table 1. TDDFT and RI-CC2 transition energies (expressed in eV) of OHBA and SA relative to the minimum of the ground state calculated at the energy minima of the S_0, S_1 and S_2 states.[a] Oscillator strengths (absorption) and lifetimes (expressed in ns) for fluorescence (fl) for vertical S1 transition are given in parentheses. Stokes shifts are marked as st

Geometry	State	B3LYP SVP/TZVP	PBE SVP	RI-CC2 SVP/TZVP	CASPT2[b]	Exptl.
OHBA						
S_0	S_1	3.92/3.94 (0.07/0.07)	3.44 (0.05)	4.15/4.10	3.74	3.9,[c],[d] 3.8 [e]
S_1 (keto)	S_1	3.53/3.51	3.09	3.48/3.38	3.22	
	0.0	3.58				
S_1 (keto)	S_0(fl)	2.71/2.66 (52.3/54.3)	2.62 (112)	2.49/2.38	2.41	2.4,[d] 2.5[c],[e]
S_1 (keto)	S_0(st)	1.21/1.28	0.82	1.66/1.72	1.33	1.5,[d] 1.4[c],[e]
SA						
S_0	S_1	4.22/4.21	3.77	4.40/4.34	3.92	3.9[f]
S_1(enol)	S_1	3.94/3.93	3.47	-		
S_1(keto)	S_1	3.93/3.93	3.47	3.93/3.83	3.46	3.69[g]
S_1 (enol)	S_0(fl)	3.56/3.58 (22.7/22.5)	3.02 (50.5)	-		
S_1(keto)	S_0 (fl)	3.03/2.95 (31.4/33.1)	3.01	2.82/2.72	2.83	2.9,[h] 2.8[f]
S_1 (enol)	S_0(st)	0.69/0.63	0.75			
S_1(keto)	S_0(st)	1.18/1.26	0.76	1.58/1.62	1.09	1.0,[f] 1.1[h]

[a]S_0: 1 ^{1}A′ (ground state); S_1: 2 ^{1}A′($\pi\pi^*$); S_2: 1 ^{1}A"($n\pi^*$).
[b]Refs. 17 and 59; [c]Ref. 60; [d]Ref. 61; [e]Ref. 62, [f]Ref. 63, [g]Ref. 64; [h]Ref. 65.

Table 2. TDDFT and RI-CC2 transition energies (expressed in eV) of HBT and HBQ relative to the minimum of the ground state calculated at the minima of the S_0, S_1 and S_2 states.[a] Oscillator strengths (adsorption) and radiative life times (expressed in ns) for fluorescence (fl) are given in parentheses. Stokes shifts are marked by st

Geometry	State	B3LYP SVP/TZVP	PBE SVP	RI-CC2 SVP/TZVP	Exptl.
HBT					
S_0	S_1	3.67/3.72 (0.34/0.36)	3.19 (0.20)	3.94/3.94	3.68[b]
S_1 (keto)	S_1	3.27/3.27	2.86	3.29/3.26	
S_1 (keto)	S_0(fl)	2.54/2.53 (17.9/18.0)	2.25 (37.9)	2.38/2.31	2.29[b]
S_1 (keto)	S_0(st)	1.13/1.19	0.94	1.56/1.63	0.93[c]
HBQ					
S_0	S_1	3.35	-	3.64	3.26[d]
S_1 (keto)	S_1	2.66	-	2.57	
S_1 (keto)	S_0(fl)	1.97	-	1.71	1.98[d]
S_1 (keto)	S_0(st)	1.13/1.19	-	1.56/1.63	

[a]S_0: 1 ^{1}A′ (ground state); S_1: 2 ^{1}A'($\pi\pi^*$); S_2: 1 ^{1}A"($n\pi^*$).
[b] Ref. 66; [c]Ref. 67; [d]Ref. 40.

the $\pi\pi^*$ state are in relatively good accordance among the three methods, with the RI-CC2 values usually in better agreement with CASPT2 and experimental results. It is noted the B3LYP and PBE radiative lifetimes values differ quite significantly. The Stokes shifts are, as expected, significant and reflect the large geometry relaxation effects occurring in the excited state.

The proton transfer curves computed at TDDFT and RI-CC2 levels of theory are presented in Figure 1 for the lowest singlet-excited $\pi\pi^*$ state of OHBA, SA and HBT.

A similar behavior is observed for the potential curves of OHBA and SA. For OHBA very shallow minima exist for the TDDFT curves with a minimum on the enol side for PBE. The B3LYP curve shows a small inflection on the enol side and a shallow minimum for

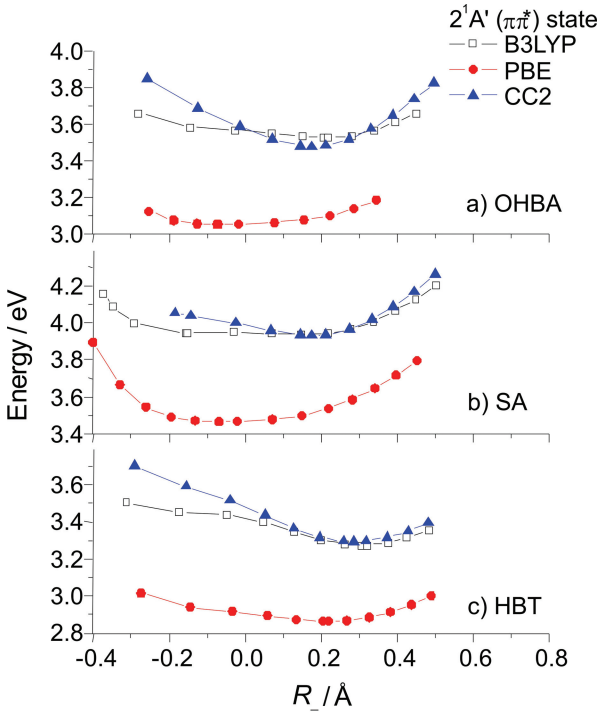

Figure 1. Proton transfer curves for OHBA, SA and HBT for the S_1 state computed with different methods.

the keto structure. The energy minimum is shifted more to the keto side and is found to be more pronounced in the RI-CC2 case as compared to the TDDFT curves. CASSCF and CASPT2 computations[17] show a similar behavior.

Figure 1 shows similar flat minima for the proton transfer curves in the ππ* state of SA. For B3LYP and PBE, two minima were found in the S_1 state whereas for RI-CC2 only one minimum is computed, which is located on the keto side and seems to be slightly more pronounced than in the TDDFT cases. Potential curves for the ππ* state of HBT are also displayed in Figure 1. A stronger predominance of the keto form is observed in comparison to the previous curves and an energy minimum is found only for the keto form. This is in contrast to CIS optimizations[56] where a pronounced minimum on the enol side was found separated by a barrier of about 2 eV from the keto form. Taking the CIS geometry the TDDFT calculations reduce considerably this barrier to about 0.1−0.2 eV. With fully consistent TDDFT calculations[39] this barrier vanishes completely. As already observed in the analysis of excitation and fluorescence data (Tables 1 and 2), the PBE proton transfer curves are also here found to be systematically too low in comparison to the other methods.

The experience obtained from the calculations described so far can be summarized as follows. Both approaches, TDDFT/B3LYP and RI-CC2 are found to reproduce the spectral properties and ESIPT processes very well. PBE underestimates the electronic excitation energies by about 0.5 eV. The general trends in the proton transfer curves are very similar for all methods and show a basically barrierless profile with the keto form slightly more stable by a few tenths of an eV in case of HBT. It is the goal of the following sections to use this experience in order to obtain an even more detailed picture of the ESIPT mechanism. Besides additional static investigations our major goal is to perform dynamics calculations in order to estimate times for the ESIPT and to analyze the coupling of the proton transfer with other molecular modes.

Table 3 presents the vertical excitation energies to the first six excited singlet states of $BP(OH)_2$ and the fluorescence energies for the mono-keto (MK) and di-keto (DK) structures starting from the S_1 state. The DK structure of $BP(OH)_2$ was found to be stable in the ground state at the RI-CC2 level. With DFT even the MK possesses a stable minimum.[57] Table 3 shows that for $BP(OH)_2$ the RI-CC2 excitations energies are somewhat higher than the corresponding TDDFT values. This trend has already been observed above. The values computed for the first excited state is in quite good agreement with the experimental absorption maximum of 3.65 eV[58], with the TDDFT results being closer to experiment than the RI-CC2 values. The second ππ* state ($2\ ^1A_g$) and the first nπ* state (1^1A_u) are located closely together at the RI-CC2 level. The next ππ* state (3^1A_g) is already higher by 0.6 eV. The situation is different at the TDDFT level where the 3^1A_g state is only 0.1 eV higher than the 2^1A_g state.

The basis set effect shown in Table 3 is quite small for TDDFT and significantly larger for RI-CC2. The fluorescence energy of the DK form agrees fairly well with the experimental result. It is noted that the relative order of the fluorescence energies for the MK and DK tautomers agrees with the experimental findings. The planar DK structure was found to be a minimum on the S_1 energy surface as verified by calculation of the harmonic vibrational frequencies. The MK structure shows pyramidalization of a bridge carbon in RI-CC2 and interring torsion in TDDFT. An energy barrier of 0.1/0.2 eV (RI-CC2/TDDFT) is located between the MK and DK S_1 minima. A shallow di-enol minimum was found at the TDDFT/B3LYP level, which disappeared when using the RI-CC2 method.

Dynamics Simulations for the ESIPT

In this section we want to concentrate the discussion on the mechanism of the ESIPT occurring in HBT and HBQ as derived from dynamics simulations. First re-

Table 3. Vertical excitation energies to the first six singlet excited states and vertical fluorescence for mono-keto (MK) and di-keto (DK) structures of $BH(OH)_2$ calculated at TDDFT/B3LYP and RI-CC2 levels of theory using different basis set. Oscillator strengths are given in parentheses, energies are expressed in eV. The symmetry used for the vertical excitations and for DK is C_{2h}, and C_s for MK

	TDDFT/B3LYP			RI-CC2		Exptl.[a]
	SVP-SV	TZVP		SVP-SV	TZVP	
$1\,^1B_u\,(\pi\pi^*)$	3.74	3.77	$1\,^1B_u\,(\pi\pi^*)$	3.90	3.85	3.65
	(0.03)	(0.03)		(0.04)	(0.04)	
$1^1A_u\,(n\pi^*)$	4.31	4.36	$2\,^1A_g\,(\pi\pi^*)$	4.69	4.61	
	(0.00)	(0.00)		(0.00)	(0.000)	
$2\,^1A_g\,(\pi\pi^*)$	4.56	4.55	$1^1A_u\,(n\pi^*)$	4.69	4.66	
	(0.00)	(0.00)		(0.00)	(0.00)	
$3\,^1A_g\,(\pi\pi^*)$	4.67	4.66	$3\,^1A_g\,(\pi\pi^*)$	5.40	5.28	
	(0.00)	(0.00)		(0.00)	(0.00)	
$2\,^1B_u\,(\pi\pi^*)$	5.06	5.04	$1\,^1B_g\,(n\pi^*)$	5.51	5.45	
	(0.01)	(0.01)		(0.00)	(0.00)	
$1\,^1B_g\,(n\pi^*)$	5.14	5.12	$2\,^1B_u\,(\pi\pi^*)$	5.62	5.49	
	(0.00)	(0.00)		(0.01)	(0.01)	
MK $(\pi\pi^*)$	2.47	2.41	MK $(\pi\pi^*)$	2.49	2.48	2.18
	(0.15)	(0.14)		(0.31)	(0.27)	
DK $(\pi\pi^*)$	2.71	2.70	DK $(\pi\pi^*)$	2.60	2.58	2.43
	(0.34)	(0.36)		(0.40)	(0.43)	

[a] Ref. 60.

sults for the double proton transfer in $BP(OH)_2$ will be discussed as well.

Figure 2 displays the time evolution within 100 fs of the R_{OH} and R_{NH} distances in HBT, HBQ, and $BP(OH)_2$ averaged over all trajectories. The time for the proton transfer was defined as the average time in which the NH and OH distances become equal. These times are 30, 36 and 10 fs for HBQ, HBT and $BP(OH)_2$, respectively. In case of HBT and HBQ these values are in very good agreement with the experimental results of 33 fs (HBT) and 25 fs (HBQ) obtained from pump-probe experiments.[40]

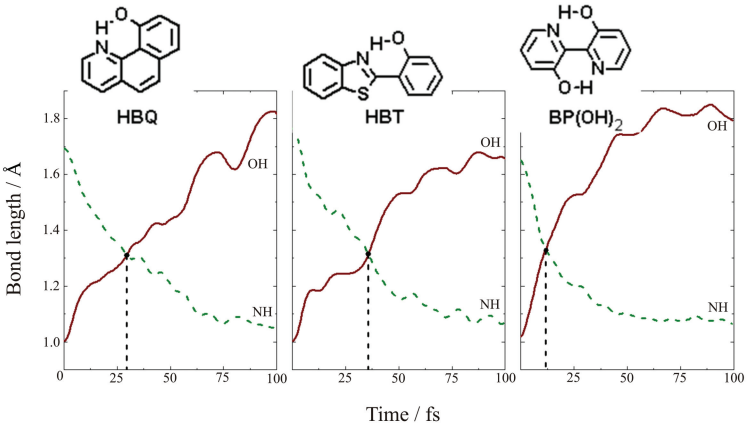

Figure 2. Time evolution of the OH and NH distances averaged over all trajectories within 100 fs for HBQ (a), HBT (b) and $BP(OH)_2$ (c).

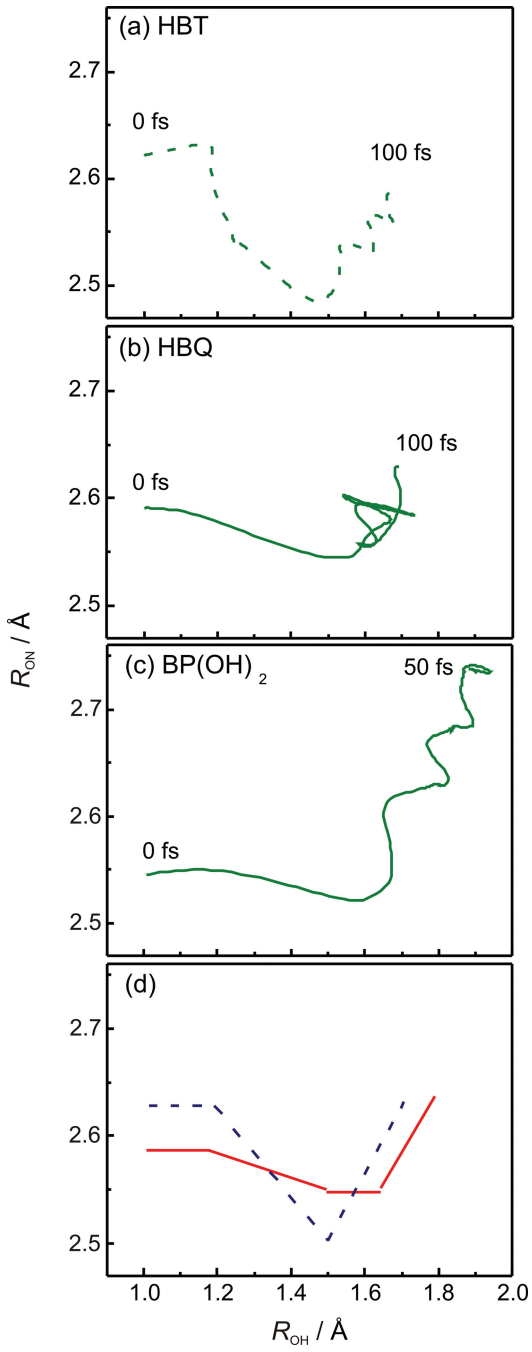

Figure 3. Average trajectory projected onto the space of the OH and NH coordinates for (a) HBT, (b) HBQ and (c) $BP(OH)_2$. Idealized sketches of the proton transfer are given in (d (full line: semi-passive, broken line: passive).

As has already been discussed before[40,41,56] the proton transfer can be described in terms of two coordinates. The first one is the OH distance and for the second one the ON distance can be chosen. This latter coordinate describes a rigid bending of the OH group toward the proton acceptor atom. Corresponding low-frequency skeletal modes involving this coordinate have been found *e.g.* in the analysis of pump-probe measurements on HBT supported by corresponding theoretical calculations. The proton transfer process can be classified quite generally into three categories:

(a) active mode – the proton transfer process is dominated by the OH-bond stretching and no skeletal distortions are involved;

(b) passive mode – the proton transfer is characterized by the skeletal distortion without significant contribution from the OH stretching.

(c) semi-passive mode – this is an intermediate case where the skeletal changes coming from the initial approach between nitrogen and oxygen atoms trigger the proton transfer.

The actual situation as derived form our dynamics simulations is shown in Figure 3 for HBT, HBQ and $BP(OH)_2$ and compared with a schematic representation. The results for HBT and HBQ will be discussed first.

It should be noted that the proton transfer sites in HBT and HBQ display strong similarities. The main difference is the rigidity with respect to skeletal motions since HBQ, in contrast to HBT, is fixed by an additional ring across the interring bond. In both cases the proton transfer starts with a stretching of the OH bond of around 0.2 Å. In case of HBT, significant decrease of the ON distance is observed bringing the proton closer to the acceptor site. This behavior is classified as passive (see also Figure 3d). As expected, in case of HBQ a somewhat different behavior is found. Only a slight decrease of the ON distance occurs justifying the classification of the ESIPT in HBQ as semi-passive.

The shape of the proton transfer process for $BP(OH)_2$ (Figure 3) in terms of the OH and ON distances looks quite similar to HBQ. Therefore it is surprising that the time for the single proton transfer to the MK form is so much shorter (10 fs) than in the other two cases (36 and 30 fs). Figure 3 shows that the initial average ON distance is significantly shorter by ~0.05 Å for $BP(OH)_2$ in comparison to HBT and HBQ. Therefore, in the former system the proton is already much closer to the proton acceptor atom and the proton transfer can proceed much faster. The reason for this reduced ON distance comes from the preparation of the initial conditions. As already explained in the section Computational Details, the initial conditions are constructed from a Wigner distribution of the quantum harmonic oscillator in terms of ground-state normal coordinates. For each OH group the respective distribution of ON distances will be symmetric around the equilibrium value. The proton transfer will occur preferentially on that OH group, which has a smaller ON distance. Thus, the proton transfer in $BP(OH)_2$ will proceed much faster since on the average always the OH group closer to the

acceptor site will show the transfer, which represents a competitive advantage over the mono-hydroxyl systems where such a possibility is absent.

This extremely fast single proton transfer in $BP(OH)_2$ has important consequences on the entire proton transfer scheme affecting especially the competition between two sequential single proton transfers as compared to one simultaneous di-proton transfer leading to the DK form. Investigation of the S_1 energy surface computed in the two OH distances shows a ridge along the symmetric stretching mode leading to an energetic stabilization of the single-proton transfer. After the fast transfer of one proton within 10 fs on the average, as discussed above, the dynamics performed for the following 100 fs can be seen as a dynamic equilibrium between the MK and DK forms. DK also appears quickly (within 10 fs) but it is typically not directly formed but rather follows through the MK intermediate. It is important to note that in spite of the asymmetric reaction scheme symmetric skeletal modes were also active as could be shown by means of a normal mode analysis of the displacement vectors computed in the course of the dynamics with respect to the reference DK structure. Recent UV-Vis transient absorption spectroscopy with 30 fs time resolution[68] report the occurrence of a concerted double proton transfer and the initial step of a sequential proton transfer within 50 fs assigning the just-mentioned symmetric modes to the concerted proton transfer. Our calculations show a much faster time scale of the initial proton transfer steps, which suggest that possibly some reinterpretation of the experimental findings has to be performed. Further investigations on these questions are in progress and will be communicated separately.[42]

CONCLUSION

Systematic review of previous investigations on the ESIPT mechanisms has been performed for several interesting cases using the TDDFT and RI-CC2 methods. Full geometry optimizations and optimized proton transfer curves were computed. Comparison with experimental absorption and fluorescence data, with available CASPT2 results and also internal comparison show that both TDDFT and RI-CC2 are well suited for the treatment of ESIPT processes. This finding has been used for detailed investigations of the ESIPT for the three systems HBT, HBQ and $BP(OH)_2$. These investigations not only included static calculations of the S_1 energy surface but also excited-state on-the-fly dynamics including all internal degrees of freedom. It has been shown that these dynamics simulations lead to a significantly deeper insight into the details of the proton transfer mechanism.

Application of these dynamics techniques to the ESIPT process in HBT and HBQ showed that the proton transfer takes place at an ultrafast time scale of 30−40 fs, in very good agreement with experimental pump-probe results. In HBT the ESIPT process is found to be promoted by skeletal deformations and, therefore, has been classified as a passive mechanism indicating that the skeletal deformations are the key modes triggering the proton transfer with the proton having a merely passive role. In the more rigid HBQ the skeletal deformations only activate the hydrogen migration mode and the OH stretch plays a more dominant role (semi-passive mode). In $BP(OH)_2$ the single proton transfer to the mono-keto form is 10 fs, significantly faster than found in the other two cases. This could be explained by the fact that on the average one of the OH groups is brought into closer contact with the proton acceptor group which facilitates the single-proton transfer to the mono-keto structure significantly. Di-keto formation starting within 10 fs proceeds through the mono-keto intermediate. Further investigations are in progress especially concerning the comparison with recent ultrafast transient absorption spectroscopy measurements.

Acknowledgements. This work was supported by the Austrian Science Fund within the framework of the Special Research Program F16 (Advanced Light Sources) and Project P18411-N19. The calculations were partially performed on the Linux cluster Schrödinger III of the computer center of the University of Vienna.

REFERENCES

1. J. Catalan, F. Fabero, M. S. Guijarro, R. M. Claramunt, M. D. S. Maria, M. D. Focesfoces, F. H. Cano, J. Elguero, and R. Sastre, *J. Am. Chem. Soc.* **112** (1990) 747−759.
2. D. Kuila, G. Kvakovszky, M. A. Murphy, R. Vicari, M. H. Rood, K. A. Fritch, J. R. Fritch, S. T. Wellinghoff, and S. F. Timmons, *Chem. Mater.* **11** (1999) 109−116.
3. P. Chou, D. Mcmorrow, T. J. Aartsma, and M. Kasha, *J. Phys. Chem.* **88** (1984) 4596−4599.
4. J. Catalan, J. Palomar, and J. L. G. dePaz, *J. Phys. Chem. A* **101** (1997) 7914−7921.
5. J. Catalan, J. L. G. dePaz, J. C. delValle, and M. Kasha, *J. Phys. Chem. A* **101** (1997) 5284−5291.
6. A. D. Roshal, A. V. Grigorovich, A. O. Doroshenko, V. G. Pivovarenko, and A. P. Demchenko, *J. Phys. Chem. A* **102** (1998) 5907−5914.
7. F. Parsapour and D. F. Kelley, *J. Phys. Chem.* **100** (1996) 2791−2798.
8. 8. F. Lahmani and A. ZehnackerRentien, *J. Phys. Chem. A* **101** (1997) 6141−6147.
9. A. O. Doroshenko, E. A. Posokhov, A. A. Verezubova, L. M. Ptyagina, V. T. Skripkina, and V. M. Shershukov, *Photochem. Photobiol. Sci.* **1** (2002) 92−99.
10. M. B. Cardoso, D. Samios, N. P. da Silveira, F. S. Rodembusch, and V. Stefani, *Photochem. Photobiol. Sci.* **6** (2007) 99−102.
11. N. Basarić and P. Wan, *J. Org. Chem.* **71** (2006) 2677−2686.
12. M. Smoluch, H. Joshi, A. Gerssen, C. Gooijer, and G. van der

Zwan, *J. Phys. Chem. A* **109** (2005) 535−541.
13. P. Toele, H. Zhang, and M. Glasbeek, *J. Phys. Chem. A* **106** (2002) 3651−3658.
14. M. Suresh, D. A. Jose, and A. Das, *Org. Lett.* **9** (2007) 441−444.
15. S. Scheiner, *J. Phys. Chem. A* **104** (2000) 5898−5909.
16. A. L. Sobolewski and W. Domcke, *Chem. Phys. Lett.* **310** (1999) 548−552.
17. A. L. Sobolewski and W. Domcke, *Phys. Chem. Chem. Phys.* **1** (1999) 3065−3072.
18. S. Mitra, R. Das, S. P. Bhattacharyya, and S. Mukherjee, *J. Phys. Chem. A* **101** (1997) 293−298.
19. A. Cembran and J. L. Gao, *Mol. Phys.* **104** (2006) 943−955.
20. A. Douhal, F. Lahmani, and A. H. Zewail, *Chem. Phys.* **207** (1996) 477−498.
21. V. Barone and C. Adamo, *Chem. Phys. Lett.* **241** (1995) 1−6.
22. J. M. Ortiz-Sanchez, R. Gelabert, M. Moreno, and J. M. Lluch, *ChemPhysChem.* **8** (2007) 1199−1206.
23. A. Migani, L. Blancafort, M. A. Robb, and A. D. Debellis, *J. Am. Chem. Soc.* **130** (2008) 6932−6933.
24. J. D. Coe, B. G. Levine, and T. J. Martinez, *J. Phys. Chem. A* **111** (2007) 11302−11310.
25. V. Guallar, V. S. Batista, and W. H. Miller, *J. Chem. Phys.* **110** (1999) 9922−9936.
26. O. K. Abou-Zied, R. Jimenez, E. H. Z. Thompson, D. P. Millar, and F. E. Romesberg, *J. Phys. Chem. A* **106** (2002) 3665−3672.
27. W. Frey and T. Elsaesser, *Chem. Phys. Lett.* **189** (1992) 565−570.
28. D. Marks, P. Prosposito, H. Zhang, and M. Glasbeek, *Chem. Phys. Lett.* **289** (1998) 535−540.
29. P. F. Barbara, P. K. Walsh, and L. E. Brus, *J. Phys. Chem.* **93** (1989) 29−34.
30. C. J. Fahrni, M. M. Henary, and D. G. VanDerveer, *J. Phys. Chem. A* **106** (2002) 7655−7663.
31. A. L. Sobolewski and W. Domcke, *J. Phys. Chem. A* **103** (1999) 4494−4504.
32. A. L. Sobolewski and W. Domcke, *Chem. Phys.* **259** (2000) 181−191.
33. S. A. do Monte, M. Dallos, T. Müller, and H. Lischka, *Coll. Czech. Chem. Commun.* **68** (2003) 447−462.
34. T. Müller, M. Dallos and H. Lischka, *J. Chem. Phys.* **110** (1999) 7176−7184.
35. F. Furche and R. Ahlrichs, *J. Chem. Phys.* **117** (2002) 7433−7447.
36. O. Christiansen, H. Koch, and P. Jorgensen, *Chem. Phys. Lett.* **243** (1995) 409−418.
37. A. Köhn and C. Hättig, *J. Chem. Phys.* **119** (2003) 5021−5036.
38. C. Hättig, *J. Chem. Phys.* **118** (2003) 7751−7761.
39. A. J. A. Aquino, H. Lischka, and C. Hättig, *J. Phys. Chem. A* **109** (2005) 3201−3208.
40. C. Schriever, M. Barbatti, K. Stock, A. J. A. Aquino, D. Tunega, S. Lochbrunner, E. Riedle, R. de Vivie-Riedle, and H. Lischka, *Chem. Phys.* **347** (2008) 446−461.
41. M. Barbatti, A. J. A. Aquino, H. Lischka, C. Schriever, S. Lochbrunner, and E. Riedle, unpublished paper.
42. F. Plasser, A. J. A. Aquino, and M. L. Barbatti, unpublished data.
43. V. Bonačić-Koutecky and R. Mitrić, *Chem. Rev.* **105** (2005) 11−65.
44. M. Barbatti, G. Granucci, M. Persico, M. Ruckenbauer, M. Vazdar, M. Eckert-Maksic, and H. Lischka, *J. Photochem. Photobiol. A: Chem.* **190** (2007) 228.
45. R. Mitrić, V. Bonačić-Koutecky, J. Pittner, and H. Lischka, *J. Chem. Phys.* **125** (2006) 164323-1-7.
46. R. Bauernschmitt and R. Ahlrichs, *Chem. Phys. Lett.* **256** (1996) 454−464.
47. R. Bauernschmitt, M. Haser, O. Treutler, and R. Ahlrichs, *Chem. Phys. Lett.* **264** (1997) 573−578.
48. A. D. Becke, *J. Chem. Phys.* **98** (1993) 5648−5652.
49. J. P. Perdew, K. Burke, and M. Ernzerhof, *Phys. Rev. Lett.* **78** (1997) 1386−1396.
50. A. Schafer, H. Horn, and R. Ahlrichs, *J. Chem. Phys.* **97** (1992) 2571−2577.
51. A. Schafer, C. Huber, and R. Ahlrichs, *J. Chem. Phys.* **100** (1994) 5829−5835.
52. C. J. Brandsen and B. H. Joachain, *Physics of Atoms and Molecules*, Longman Group Limited, 1983.
53. R. Ahlrichs, M. Häser, M. Horn, and C. Kölmel, *Chem. Phys. Lett.* **162** (1989) 165−169.
54. M. Barbatti, G. Granucci, H. Lischka, M. Ruckenbauer, and M. Persico, *NEWTON-X: a package for Newtonian dynamics close to the crossing seam*, version 0.14b, 2007. www.univie.ac.at/newtonx
55. A. L. Sobolewski, W. Domcke, and C. Hättig, *J. Phys. Chem. A* **110** (2006) 6301−6306.
56. R. de Vivie-Riedle, V. De Waele, L. Kurtz, E. Riedle, *J. Phys. Chem. A* **107** (2003) 10591−10599.
57. R. Gelabert, M. Moreno, and J. M. Lluch, *ChemPhysChem.* **5** (2004) 1372−1378.
58. H. Zhang, P. van der Meulen, and M. Glasbeek, *Chem. Phys. Lett.* **253** (1996) 97−102.
59. A. L. Sobolewski and W. Domcke, *Chem. Phys.* **184** (1994) 115−124.
60. S. Nagaoka, N. Hirota, M. Sumitani, K. Yoshihara, E. Lipczynskakochany, and H. Iwamura, *J. Am. Chem. Soc.* **106** (1984) 6913−6916.
61. S. Nagaoka and U. Nagashima, *Chem. Phys.* **136** (1989) 153−163.
62. M. A. Morgan, E. Orton, and G. C. Pimentel, *J. Phys. Chem.* **94** (1990) 7927−7935.
63. D. D. Pant, H. C. Joshi, P. B. Bisht, and H. B. Tripathi, *Chem. Phys.* **185** (1994) 137−144.
64. T. Nishiya, S. Yamauchi, N. Hirota, M. Baba, and I. Hanazaki, *J. Phys. Chem.* **90** (1986) 5730−5735.
65. F. Lahmani and A. ZehnackerRentien, *Chem. Phys. Lett.* **271** (1997) 6−14.
66. S. Lochbrunner, A. J. Wurzer, and E. Riedle, *J. Chem. Phys.* **112** (2000) 10699−10702.
67. S. Lochbrunner, A. J. Wurzer, and E. Riedle, *J. Phys. Chem. A* **107** (2003) 10580−10590.
68. K. Stock, C. Schriever, S. Lochbrunner, and E. Riedle, *Chem. Phys.* **349** (2008) 197.

SAŽETAK

Ultrabrzi proton transfer procesi u pobuđenom stanju: energetske površine i simulacije dinamike procesa u letu[§]

Adélia J. A. Aquino, Felix Plasser, Mario Barbatti i Hans Lischka

Institute for Theoretical Chemistry, University of Vienna Waehringerstrasse 17, A-1090 Vienna, Austria

Revidirani su intramolekularni prijenosi protona u pobuđenom stanju (engl. *the excited-state intramolecular proton transfer*, ESIPT) za nekoliko probnih sistema [*o*-hidroksibenzaldehid (OHBA), salicilna kiselina i 2-(2´-hidroksifenil)-benzotiazol (HBT)] s ciljem provjere primjenjivosti vremenski ovisne DFT metode (engl. *time dependent density functional theory*, TDDFT) i postupka razlučivanja identiteta aproksimativnom metodom spregnutih grozdova drugog reda (engl. *Resolution-of-the-identity approximate second-order coupled cluster method*, RI–CC2). Pokazano je da su ovi pristupi pogodni za opis ESIPT procesa. Usporedna analiza prethodnih i novih simulacija dinamike procesa u pobuđenom stanju provedena je za HBT, 10-hidroksibenzo[*h*]kinolin (HBQ) i [2,2´-bipridil]-3,3´-diol ($BP(OH)_2$). Vremenska skala za ESIPT proces u ovim sistemima nalazi se u intervalu od 30–40 fs za HBT i HBQ, te oko 10 fs za reakciju prijenosa prvog protona u $BP(OH)_2$. Simulacije dinamike također pokazuju da je prijenos protona u HBT jako spregnut s vibracijama kostura molekule, te da proton igra prilično pasivnu ulogu, dok je u HBQ pronađen polu-pasivni mehanizam radi povećane rigidnosti molekule u usporedbi sa HBT. Prodiskutirana je također i specijalna uloga dvostrukog prijenosa protona u $BP(OH)_2$.

[§] Simulacije dinamike u letu (engl. *On-the-fly dynamics simulations*)